J Mater Sci (2009) 44:6035–6039
DOI 10.1007/s10853-009-3822-z

Synthesis and mechanical behavior of ternary Mg–Cu–Dy in situ bulk metallic glass matrix composite

X. F. Wu · Y. Si · Z. Y. Suo · Y. Kang · K. Q. Qiu

Received: 2 June 2009 / Accepted: 18 August 2009 / Published online: 10 September 2009

Abstract In situ Mg phase reinforced $Mg_{70}Cu_{17}Dy_{13}$ bulk metallic glass (BMG) matrix composite with diameter of 3 mm was fabricated by conventional Cu-mold casting method. The results show that the Mg-based BMG matrix composite exhibits some work hardening except for initial elastic deformation, a high fracture compressive strength of 702 MPa, which is 1.125 times higher than single-phase $Mg_{60}Cu_{27}Dy_{13}$ BMG and some plastic strain of 0.81%. The improvement of the mechanical properties is attributed to the fact that the Mg phase distributed in the amorphous matrix of the alloy has some effective load bearing and plastic deformation ability to restrict the expanding of shear bands and cracks and produce its own plastic deformation, which was proved by the shear deforming and fracturing mode and the fracture surfaces characterized by the vein pattern, severe remelting, and the very rough and bumpy region of the alloy.

Introduction

Over the last nearly two decades, many bulk metallic glasses (BMGs) with good glass forming ability have been developed due to their fundamental scientific importance and engineering application potential. In terms of mechanical properties, BMGs exhibit higher strength and hardness, larger elastic strain limit, and better wear resistance. However, BMGs fail catastrophically on one dominant shear band after elastic deformation without distinct plastic strain, especially under tensile or compressive load, which limits their potential as engineering materials. To improve the plasticity of the monolithic BMGs, BMG matrix composites reinforced with ex situ ductile metals or refractory ceramics particles and in situ precipitated dendritic or crystalline particles phase have already been found and they exhibit higher fracture strength and plastic deformation than those of their corresponding single phase BMG [1–8]. Mg-based BMGs were paid more and more attention because of their low density, high specific strength, and relatively low cost, which can provide the possibility to obtain new light alloys for structural applications. However, Mg-based BMGs are more brittle than other BMGs even fail in the elastic regime with no observable plasticity. In order to overcome this drawback, ex situ TiB_2 [9, 10], SiC [11], and Nb [12] particulate, and in situ α-Fe solid solution precipitate [13] reinforced Mg–Cu–Zn–Y, Mg–Cu–Ag–Gd, and Mg–Cu–Ni–Zn–Ag–Y BMG matrix composites were prepared, which improves the strength or plastic strains of these alloys to different extents. Based on our preliminary work in which Mg–Cu–Dy BMG with 8-mm diameter was prepared (a separate article will be published), ternary Mg–Cu–Dy BMG matrix composite reinforced with in situ Mg precipitated phase was prepared by conventional Cu-mold casting method. This article intends to present the structure, the mechanical properties, and the deformation and fracture behavior of the composite.

Experimental procedure

Ingots with nominal composition of $Mg_{87-x}Cu_xDy_{13}$ ($x = 17, 27, 37$ at.%) alloys were prepared by arc melting

X. F. Wu (✉) · Y. Si · Y. Kang
School of Materials and Chemical Engineering, Liaoning University of Technology, 169 Shiying Street, 121001 Jinzhou, People's Republic of China
e-mail: hgd901@126.com

Z. Y. Suo · K. Q. Qiu
School of Materials Science and Engineering, Shenyang University of Technology, 58 South Xinghua Street, 110023 Shenyang, People's Republic of China

the mixture of pure metals (Mg, Cu, and Dy) with a purity of more than 99.9% under a Ti-gettered Ar atmosphere. To ensure homogeneity of the samples, the ingots were remelted several times. Fifty-millimeter length cylindrical rods with different diameters were prepared by pouring liquid metal, which was melted using induction furnace, through a quartz nozzle into a copper mold under certain argon pressure as well as purified argon atmosphere. The structure of samples was detected by X-ray diffraction (XRD) pattern by using a Rigaku X-ray diffractometer (Cu–K_α radiation). Compression experiments were carried out on a MTS-type axial–torsional load frame at room temperature. The samples with an aspect ratio of 2:1 were prepared for the compressive testing. The compressive strain rate was 3.0×10^{-4} s^{-1}. JEOLJSM6301 scanning electron microscope (SEM) was used for the analysis of the as-cast morphologies and fracture features. Six rods of the same diameter and composition for every alloy composite were compressed and analyzed.

Results

Figure 1 shows the XRD patterns of the cast rods with diameter of 3 mm of $Mg_{87-x}Cu_xDy_{13}$ ($x = 17, 27, 37$ at.%) alloys. The XRD patterns from the alloy $x = 27$ consists only of a broad peak, with no evidence of any crystalline Bragg peaks within the detectable limitation of the XRD, while a few sharp diffraction peaks corresponding to crystalline phases superimposed on the broad amorphous peaks are observed for the other two alloys, indicating that $Mg_{60}Cu_{27}Dy_{13}$ alloy is fully amorphous, and $Mg_{70}Cu_{17}Dy_{13}$ and $Mg_{50}Cu_{37}Dy_{13}$ alloys are partially amorphous with a significant fraction of crystalline phases. The crystalline phase existing in the $Mg_{50}Cu_{37}Dy_{13}$ and $Mg_{70}Cu_{17}Dy_{13}$ alloys were identified as $DyMg_x$ and Mg phases, respectively. The volume fraction of the $DyMg_x$ in the $Mg_{50}Cu_{37}Dy_{13}$ and Mg phase in the $Mg_{70}Cu_{17}Dy_{13}$ are 13.6 and 11.2 vol.%, respectively. In addition, very small amount dysprosium oxides exists in the $Mg_{70}Cu_{17}Dy_{13}$ alloy.

A series compression tests were conducted on three as-cast Mg-based alloys. Figure 2 shows the quasistatic compressive stress–strain curves at room temperature for the as-cast $Mg_{87-x}Cu_xDy_{13}$ rods with a diameter of 3 mm and a length of 6 mm. As other metallic glasses, the curves of the $Mg_{60}Cu_{27}Dy_{13}$ and $Mg_{50}Cu_{37}Dy_{13}$ alloys only display an initial elastic deformation behavior with almost no plasticity at room temperature, however, there is a significantly difference in the values of fracture strength. The fracture strength of $Mg_{50}Cu_{37}Dy_{13}$ alloy only is 368 MPa, while one of the $Mg_{60}Cu_{27}Dy_{13}$ alloy reaches 624 MPa. On the other hand, $Mg_{70}Cu_{17}Dy_{13}$ alloy exhibits initial elastic deformation, followed by yielding, plastic deformation, and finally fracture under compressive loading. The samples exhibit yield strength of 561 MPa and fracture strength of 702 MPa, which reveals some work hardening during the end of the deformation process. The plastic strain of the samples is about 0.81%. Initial non-linear parts on the curves of three alloys were resulted from the systematic error of the compression machine, which results in larger elastic strains.

Figure 3 shows the morphology of the fractured specimen of the three alloys under uniaxial compressive loading. The $Mg_{50}Cu_{37}Dy_{13}$ alloy shattered into fragments longitudinally easily, the fracture direction is parallel to the compressive loading axis during compressive test (Fig. 3a), while the lower portion of the fractured samples of the

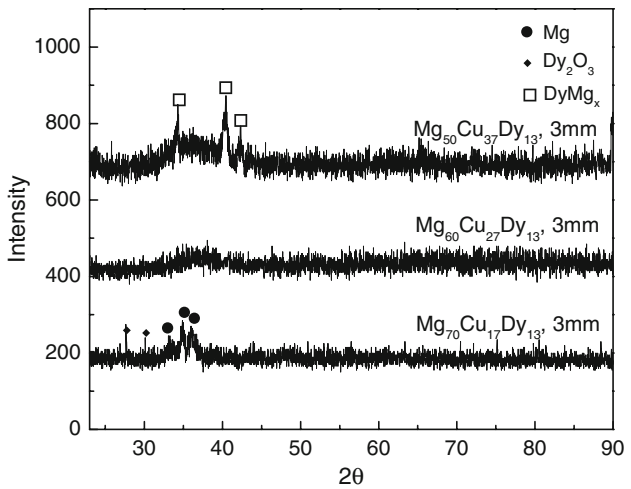

Fig. 1 The XRD patterns for $Mg_{87-x}Cu_xDy_{13}$ ($x = 17, 27, 37$ at.%) alloys

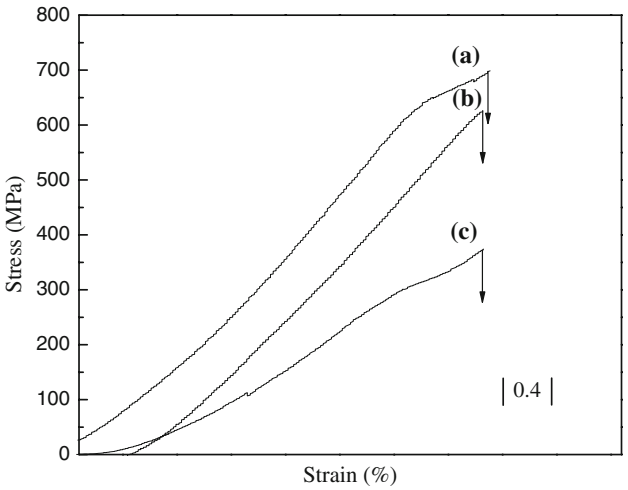

Fig. 2 The stress–strain curves of $Mg_{87-x}Cu_xDy_{13}$ ($x = 17, 27, 37$) alloys: (*a*) $x = 17$, (*b*) $x = 27$, and (*c*) $x = 37$

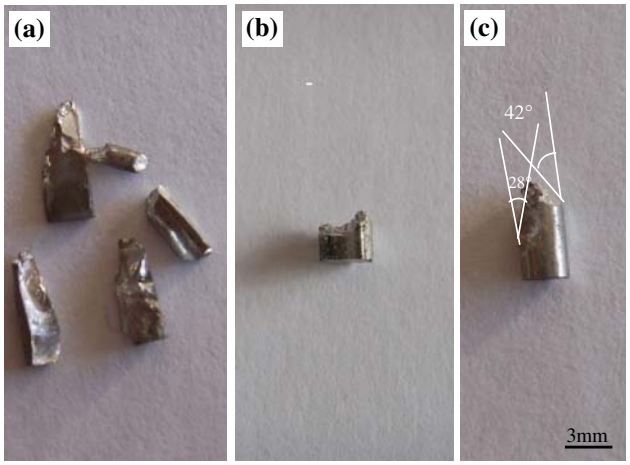

Fig. 3 Morphology of the fracture surfaces of **a** $Mg_{50}Cu_{37}Dy_{13}$, **b** $Mg_{60}Cu_{27}Dy_{13}$, **c** $Mg_{70}Cu_{17}Dy_{13}$ alloys

$Mg_{60}Cu_{27}Dy_{13}$ alloy remained as a whole piece and the fracture direction is perpendicular to the compressive loading axis (Fig. 3b). For the $Mg_{70}Cu_{17}Dy_{13}$ alloy, there are two fracture surfaces, which are inclined under an angle θ to the stress axis and can be measured as marked in the figures. The fracture angles θ between the stress axis and the fracture surfaces (shear planes) are equal to 42° and 28°, respectively (Fig. 3c), indicating dominance of shear stress in the failure process.

Figure 4 shows the SEM micrographs of the fracture surfaces of the $Mg_{50}Cu_{37}Dy_{13}$ and $Mg_{60}Cu_{27}Dy_{13}$ alloys. The $Mg_{50}Cu_{37}Dy_{13}$ alloy fractures in brittle features, some crystals disperse in a planar and smooth matrix and most are broken (Fig. 4a). For the $Mg_{60}Cu_{27}Dy_{13}$ alloy, no crystals are seen and the fracture surface is also planar and smooth, which is the classical characteristic of fracture surface of Mg-based BMGs.

The $Mg_{70}Cu_{17}Dy_{13}$ alloy exhibits a very different fracture surfaces, On the whole 42° fracture surface, typical well-developed veins can be observed and the veins have an obvious direction from right to left as marked by arrows (Fig. 5a). Also it can be noticed that some shear bands appeared near the fracture surface on the outside surface of the sample (Fig. 5b). Figure 6 shows the morphology of 28° fracture surface of $Mg_{70}Cu_{17}Dy_{13}$ alloy. The fracture surface consists of region I, region II, and region III, which are located in the top, the middle part, and the bottom of the fracture surface, respectively (Fig. 6a). In the region I, vein patterns are observed, accompanied by local melting appearing as evidenced by the formation of "liquid droplets" during loading, as shown in the Fig. 6b, c. These phenomena very often appear in monolithic ductile BMGs such as Zr-based BMG [10]. Compared to the BMGs, however, veins are undeveloped and the fracture surface is like a slurry flow, in addition, the liquid droplets are larger. It appears that the crystalline phases embedded in the glassy matrix make the temperature in the shear band become higher enough to cause the matrix to show more distinct viscous flow. The region II is characterized by

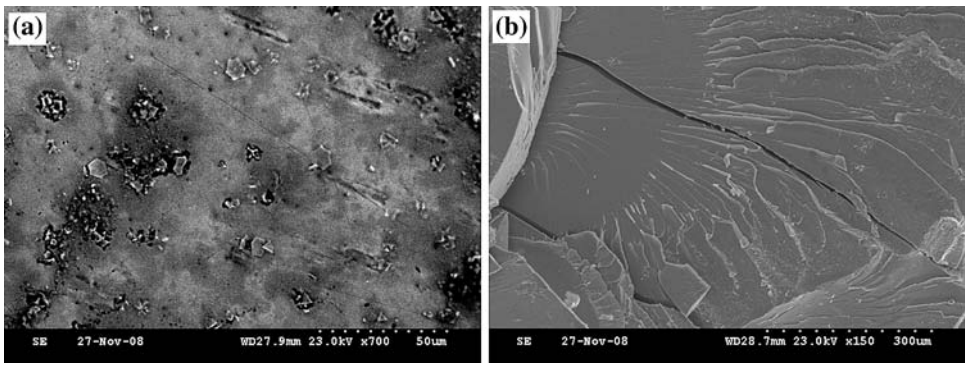

Fig. 4 SEM micrographs of the fracture surface of **a** $Mg_{50}Cu_{37}Dy_{13}$, **b** $Mg_{60}Cu_{27}Dy_{13}$ alloys

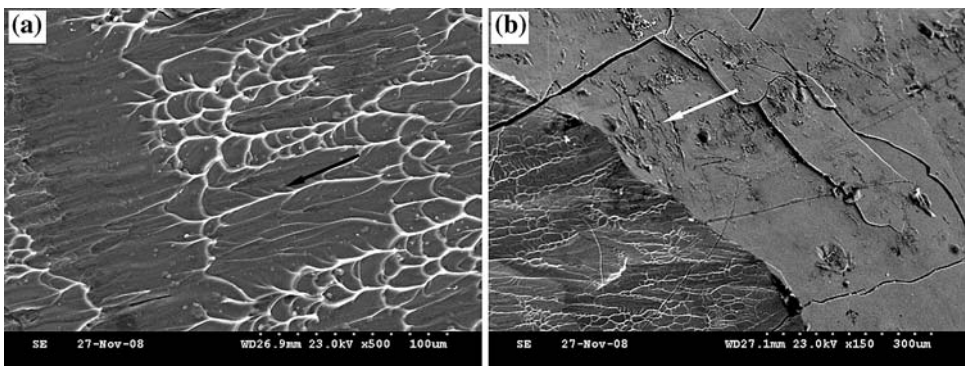

Fig. 5 **a** SEM micrographs of the 42° fracture surface and **b** shear bands on outside surface of $Mg_{70}Cu_{17}Dy_{135}$ alloy

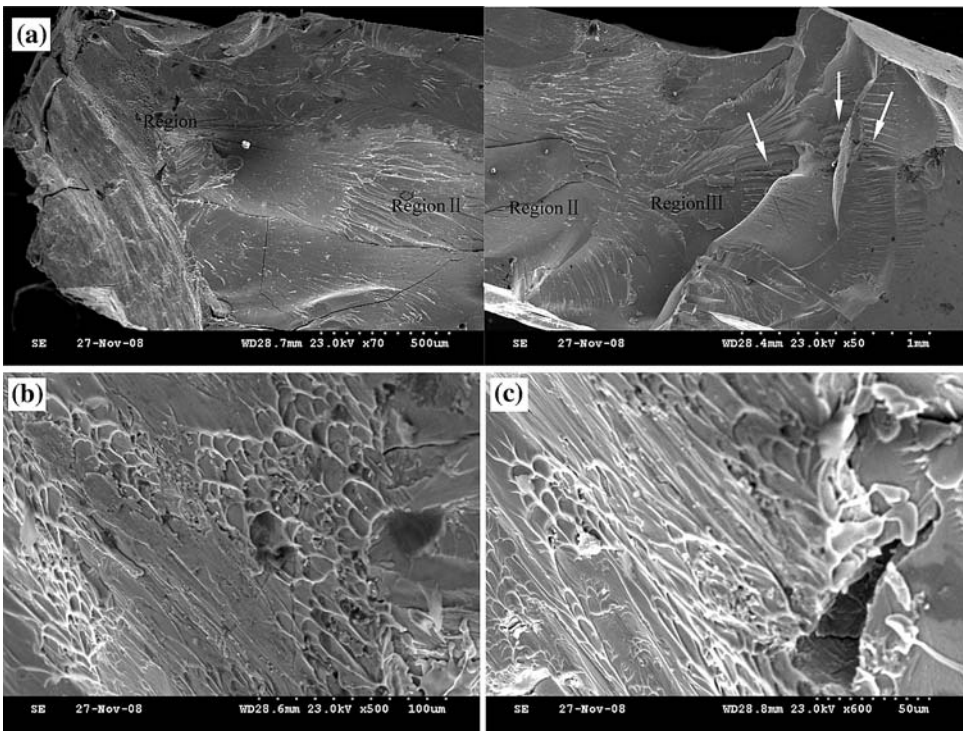

Fig. 6 Morphology of 28° fracture surface of $Mg_{70}Cu_{17}Dy_{13}$ alloy **a** region I, II, and III; **b** vein patterns in region I; **c** "liquid droplets" in region I

planar and smooth surface (Fig. 6a), which is similar to monolithic Mg-based BMGs. In the region III, the fracture surface is very rough and bumpy, and there are some big grooves, as seen in the right part of Fig. 6a.

Discussion

Traditional opinion considers that the deformation and fracture of all amorphous alloys take place by inhomogeneous shear sliding. As the deformation of the amorphous alloys concentrates on one or several shear bands and the other shear bands do not experience much deformation, unceasing deformation occurs and promotes further work-softening in one or several shear bands [14], finally leading to high fracture strength and catastrophic failure without obvious plastic strain and remaining fracture surface consists of a well-developed vein pattern and molten droplets. Above $Mg_{60}Cu_{27}Dy_{13}$ BMG and some Mg-based BMGs prepared previously [10, 11, 15] show that Mg-based monolithic BMGs do not deform and fracture in shear mode. Upon failure, the samples of the BMGs shatter into pieces or are crushed into fragments, resulting in their premature failure before reaching its elastic limit and lower strength. Recently, Xi [16] found that there is a dimple structure at the fracture surface indicating some type of "ductile" fracture mechanism in the brittle glasses. It can be expected that as long as the mode of the deformation and fracture of Mg-based BMGs is changed into shear one and the propagation of individual shear bands is confined, their strength and plasticity can be improved, which has been proved by the addition of SiC, TiB_2, and Nb particles into some Mg-based BMGs [8–11]. The effect of such BMG matrix composites reinforced with ex situ or in situ crystalline phases on the mechanical properties, the deformation, and fracture mode depends on the nature, size, volume fraction, and distribution of the phases, especially phase nature. The broken $DyMg_x$ phase observed in the fracture surfaces of the $Mg_{50}Cu_{37}Dy_{13}$ (Fig. 4a) indicates that the phase is brittle as it belongs to intermetallic crystallites and does not yield large loading. When small uniaxial compression loading exerts on the sample of the material, the phase first cracks due to the absence of its plastic deformation such as dislocation motion and twinning. Consequently, the stress intensity in the amorphous region bounded on the tip of the cracks of the broken crystallites increases, rapid crack propagation takes place by spanning the tip and the samples shatter into fragments longitudinally (Fig. 3a), leading to the very low fracture strength of the whole composite (Fig. 2), which is similar to the embrittlement in the Zr-based amorphous matrix composites including the quenched-in nanocrystals when the volume fraction of these nanocrystals is up to 10 vol.% although the size of the crystals is very small [17]. For the $Mg_{70}Cu_{17}Dy_{13}$ alloy, the fracture angle close to 45° and the presence of the vein pattern and remelting on the fracture surface indicates that the deformation and fracture behavior of the alloy are dominated by the shear fracture. Moreover,

the fracture surfaces characterized by the more viscous slurry-like flow layer (Fig. 6b) and the larger liquid droplets (Fig. 6c) considered as severe remelting for the alloy, and the very rough and bumpy fracture surface and some big grooves in the region III (Fig. 6a) reveal that the crystalline phase precipitated during solidification, i.e., Mg phase embedded in the glassy matrix are not brittle due to its simple body cubic structure, do not crack prematurely after yielding large loading, then retard the formation and the expansion of main shear band and increases the viscosity of its flow, resulting in a significant increase of energy release during fracture. This is in agreement with a large increase in fracture strength of the alloy and a higher value than $Mg_{60}Cu_{27}Dy_{13}$ monolithic BMGs, as seen in Fig. 2. On the other hand, ductile Mg phase was assured to contribute to the strain-hardening of the materials by dislocation motion, twinning, and phase transformation induced plasticity. Furthermore, the presence of the ductile phase can seed the initiation of organized shear band patterns, confine the propagation of individual shear bands and trigger the formation of multiple shear bands (Fig. 5b). Therefore, plasticity is distributed more homogeneously in the shear band patterns, which results in some strain to failure of the composite.

Conclusion

In summary, in situ Mg phase reinforced $Mg_{70}Cu_{17}Dy_{13}$ BMG matrix composite with a diameter of 3 mm was fabricated by conventional Cu-mold casting method. The composite exhibits initial elastic deformation, followed by yielding, work hardening (plastic deformation), and finally fracture under compressive loading. The fracture compressive strength of the composite reaches 702 MPa, which is 1.125 times higher than the single-phase $Mg_{60}Cu_{27}Dy_{13}$ BMG. The plastic strain of the composite is about 0.81%. The deformation and fracture of the composite mainly occurs in a shear mode and the fracture surface is characterized by the vein pattern, severe remelting, and the some very rough and bumpy region. A high fracture strength and some plasticity are attributed to the fact that the Mg phase distributed in the amorphous matrix of the alloy has some effective load bearing and plastic deformation ability, which leads to a positive effect on the improvement of fracture strength and plasticity by restricting the expanding of shear bands and cracks and producing its own plastic deformation.

Acknowledgements Funding by the Natural Science Foundation of Liaoning Province under Grant No. 20032137 is gratefully acknowledged.

References

1. Dandliker RB, Conner RD, Johnson WL (1998) J Mater Res 13:2896
2. Wang G, Shen J, Qin QH, Sun JF, Stachurski ZH, Zhou BD (2005) J Mater Sci 40:4561. doi:10.1007/10853-005-3081-6
3. Hays CC, Kim CP, Johnson WL (2000) Phys Rev Lett 84:2901
4. Hu X, Ng SC, Li Y (2003) Acta Mater 51:561
5. Kinaka M, Kato H, Hasegawa M, Inoue A (2008) Mater Sci Eng A494:299
6. Scudino S, Surreddi KB, Sager S (2008) J Mater Sci 43:4518. doi:10.1007/s10853-008-2647-5
7. Sun YF, Todaka Y, Umemoto M (2008) J Mater Sci 43:7457. doi:10.1007/s10853-008-2634-x
8. Singh D, Yadav TP, Tiwari RS (2009) J Mater Sci 44:3883. doi:10.1007/s10853-009-3530-8
9. Xu YK, Xu J (2003) Scr Mater 49:843
10. Xu YK, Ma H, Xu J, Ma E (2005) Acta Mater 53:1857
11. Li J, Wang L, Zhang HF, Hua ZQ, Cai HN (2007) Mater Lett 61:2217
12. Pan DG, Zhang HF, Wang AM, Hu ZQ (2006) Appl Phys Lett 89:1904
13. Ma H, Xu J, Ma E (2003) Appl Phy Lett 83:2372
14. Subhash G, Dowding RJ, Kecskes LJ (2002) Mater Sci Eng A334:33
15. Chen G, Ferry M (2006) J Mater Sci 41:4643. doi:10.1007/s10853-006-0059-y
16. Xi XK, Zhao DQ, Pan MX, Wang WH, Wu Y (2005) Phys Rev Lett 94:125510
17. Bian Z, Chen GL, He G, Hui XD (2001) Mater Sci Eng 316A:135